Electronic Supplementary Material (ESI) for Journal of Materials Chemistry A.
This journal is © The Royal Society of Chemistry 2024

Interface Engineering and Oxygen Vacancy Derived from Plasma-treated Cu_2O Synergistically Enhancing Electrocatalytic CO_2-to-C_{2+} Conversion

Lei Wang, [1,2Δ] *Xue Yao,* [3Δ]*Subhajit Jana,* [1Δ]*Yongzan Zhou,* [1Δ] *Chunlan Qin,* [4]*Hongwei Shou,* [4] *Youchao Teng,* [1] *Ning Chen,* [5] *Lidong Zhang,* [3] *Chandra Veer Singh,*[3,6*]*Zhongchao Tan,*[1,7*] *Yimin A. Wu*[1,2,8 *]

[1]Department of Mechanical and Mechatronics Engineering, University of Waterloo, Waterloo, Ontario N2L 3G1, Canada

[2]Waterloo Institute for Nanotechnology, University of Waterloo, Waterloo, Ontario N2L 3G1, Canada

[3]Department of Materials Science and Engineering, University of Toronto, Toronto, Ontario M5S 3E4, Canada

[4]National Synchrotron Radiation Laboratory, University of Science and Technology of China, Hefei 230029, P. R. China;

[5]Canadian Light Source, Saskatoon, SK S7N 2V3, Canada

[6]Department of Mechanical and Industrial Engineering, University of Toronto, Toronto, Ontario M5S 3G8, Canada

[7]Eastern Institute of Technology, No. 568 Tongxin Road, Zhenhai District, Ningbo, Zhejiang, 315200, China

[8]Department of Chemistry, University of Waterloo, Waterloo, Ontario N2L 3G1, Canada

[Δ] Equal contributions

* Corresponding emails: chandraveer.singh@utoronto.ca; ztan@eitech.edu.cn; yimin.wu@uwaterloo.ca

This supplementary information includes: Figure S1 to S12 and Table S1-3.

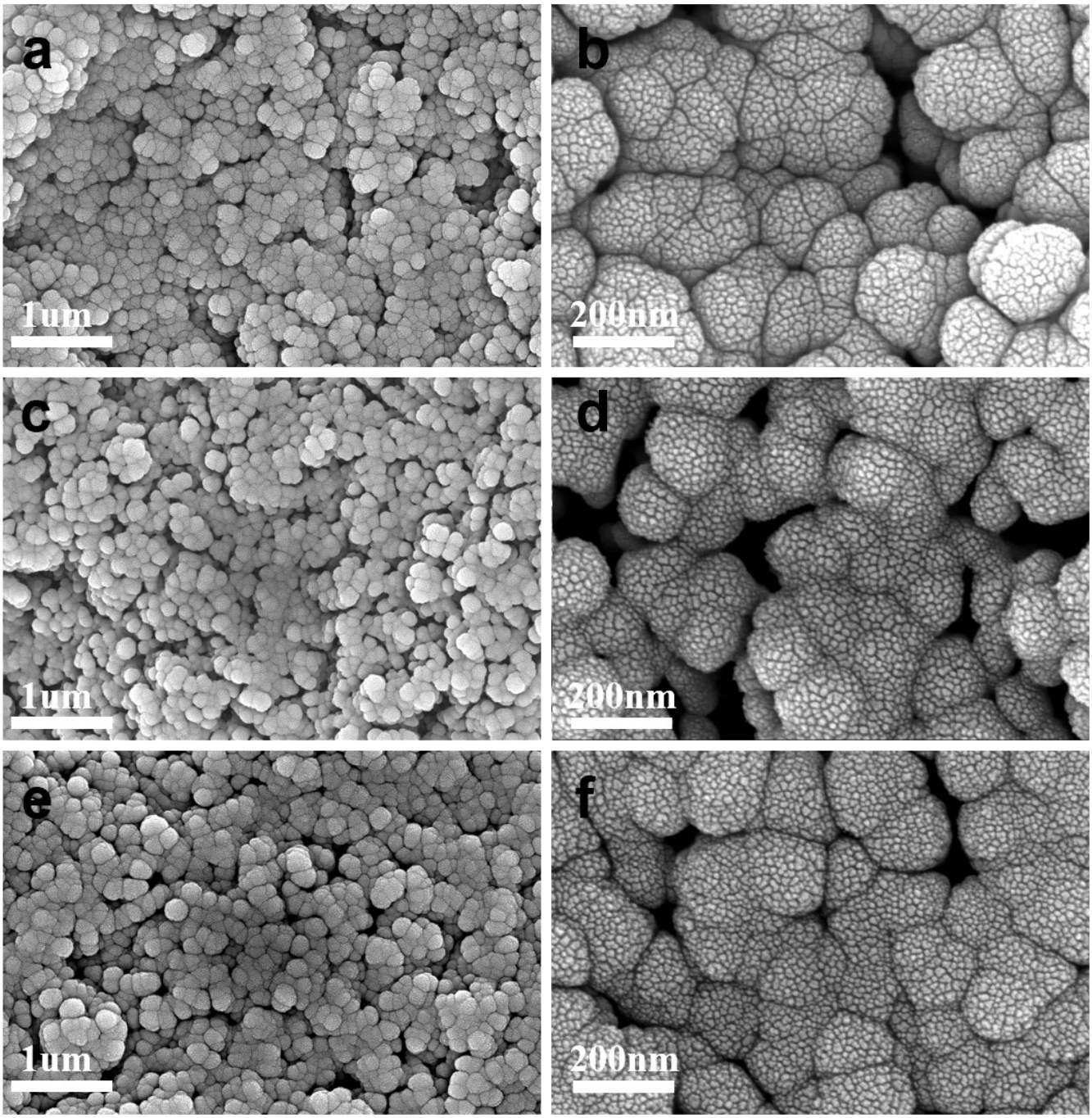

Figure S1. (a-f) SEM images of Cu_2O (a-b), Cu_2O-Ar/H_2 (c-d) and Cu_2O-Ar/O_2 (e-f).

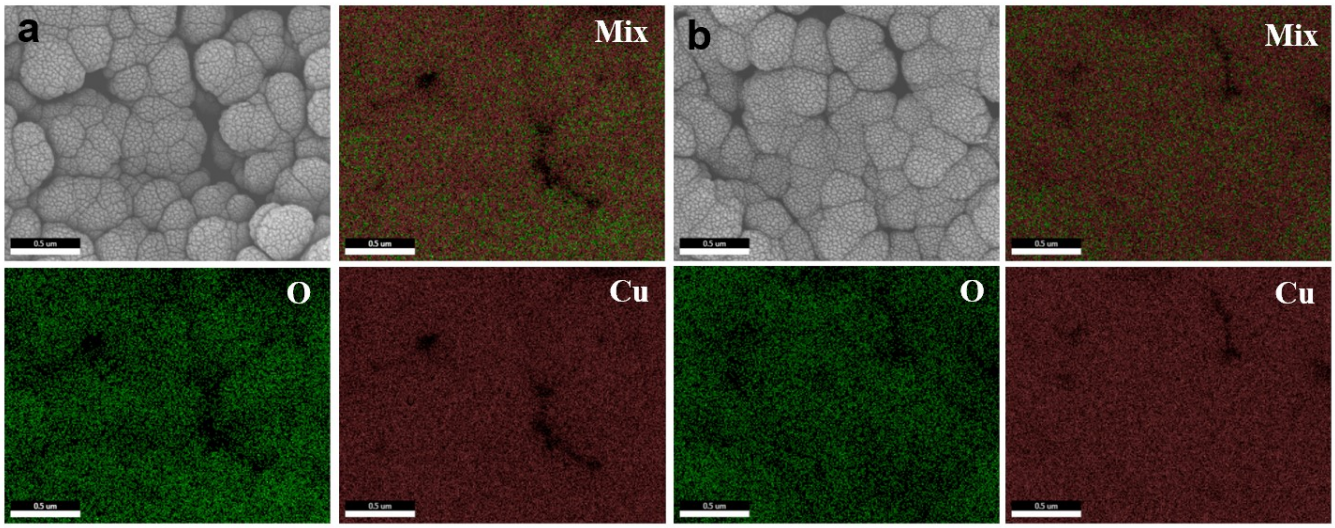

Figure S2. (a-b) SEM-EDS elemental mapping images of Cu_2O (a) and Cu_2O-Ar/O_2 (b).

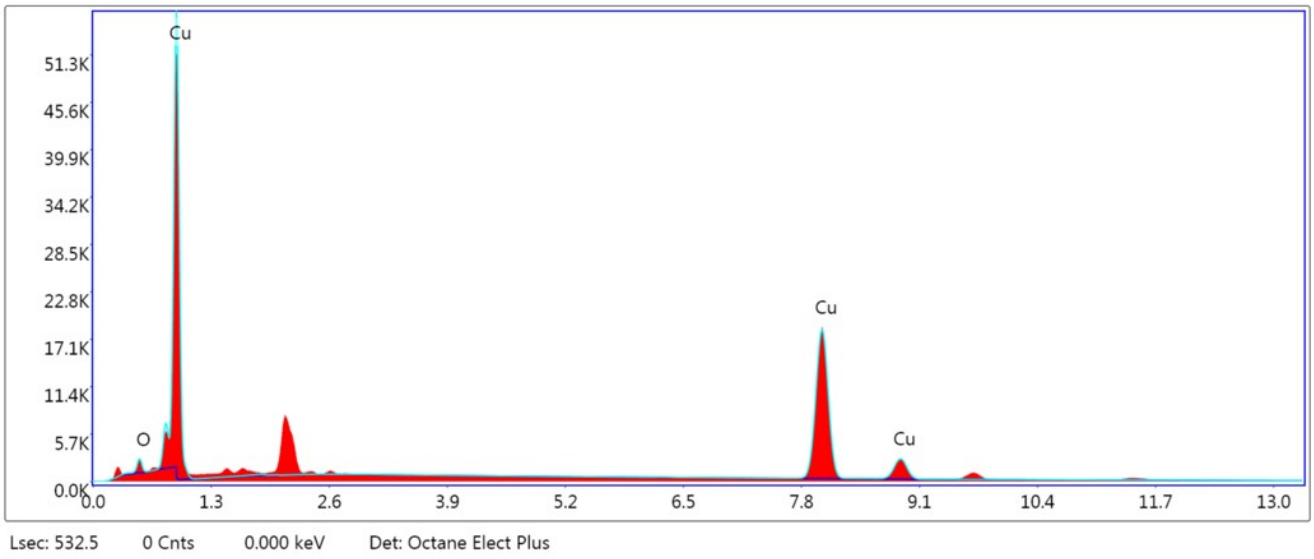

Element	Weight %	Atomic %	Net Int.	Error %	Kratio
O K	2.50	9.24	38.90	9.60	0.0105
Cu K	97.50	90.76	1102.10	1.75	0.9670

Figure S3. (a) Element content distribution of Cu_2O-Ar/H_2.

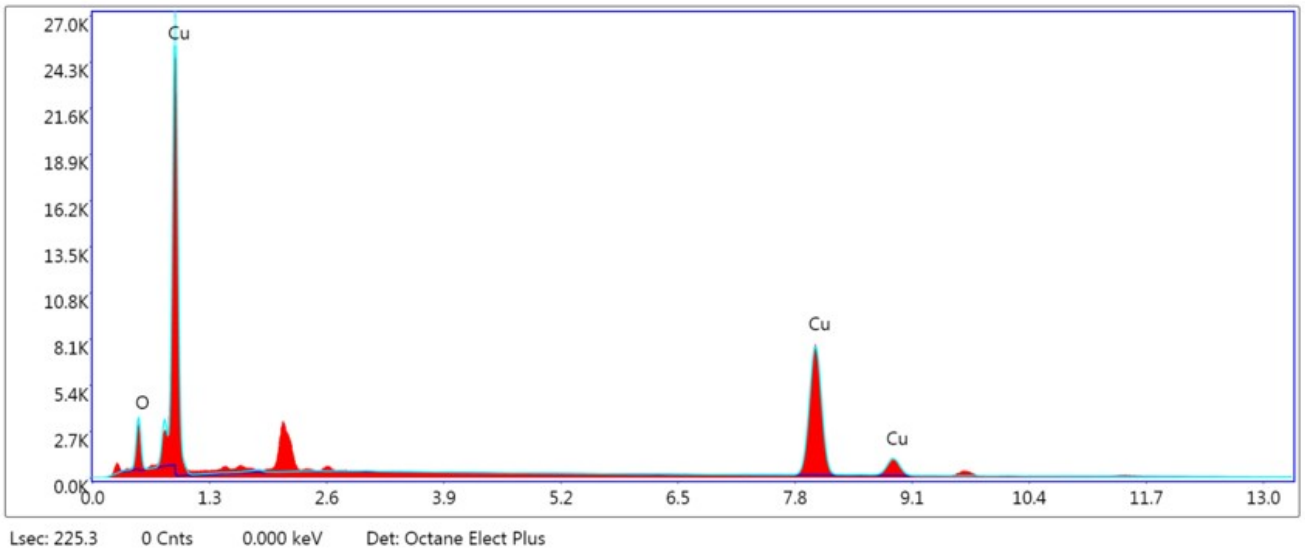

Element	Weight %	Atomic %	Net Int.	Error %	Kratio
O K	14.56	40.37	158.20	8.85	0.0646
Cu K	85.44	59.63	615.00	2.28	0.8151

Figure S4. (a) Element content distribution of Cu_2O.

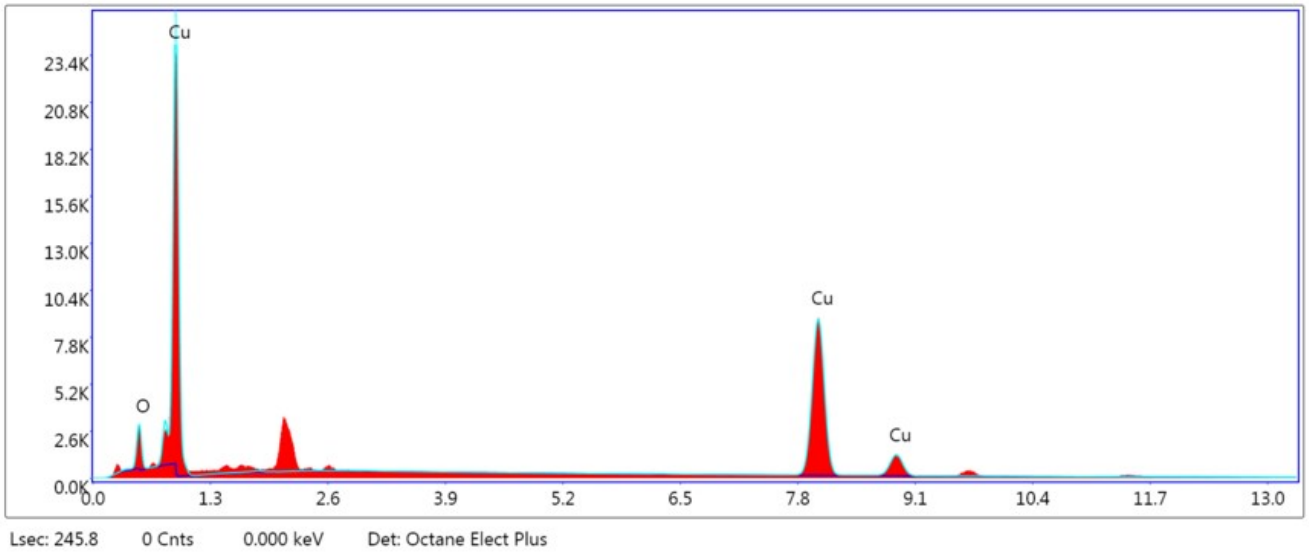

Element	Weight %	Atomic %	Net Int.	Error %	Kratio
O K	12.07	35.28	123.40	9.15	0.0529
Cu K	87.93	64.72	607.10	2.32	0.8456

Figure S5. (a) Element content distribution of Cu_2O-Ar/O_2.

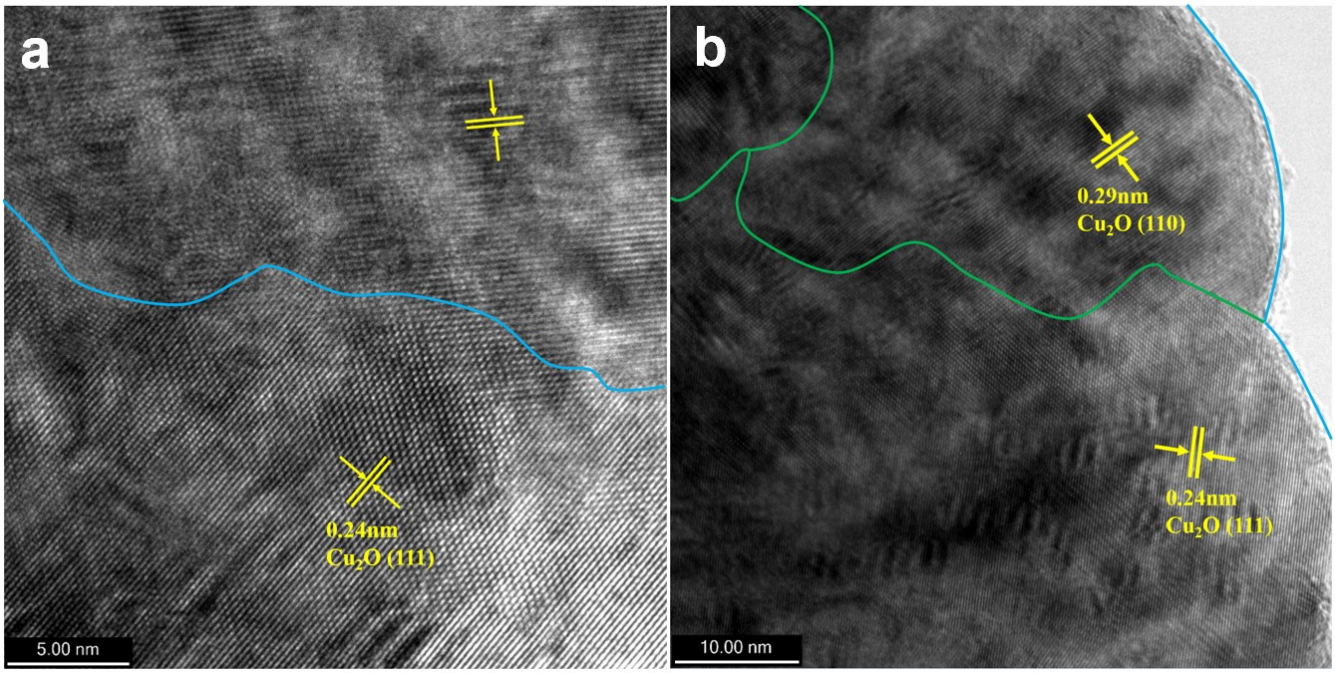

Figure S6. (a-b) HRTEM images of Cu_2O.

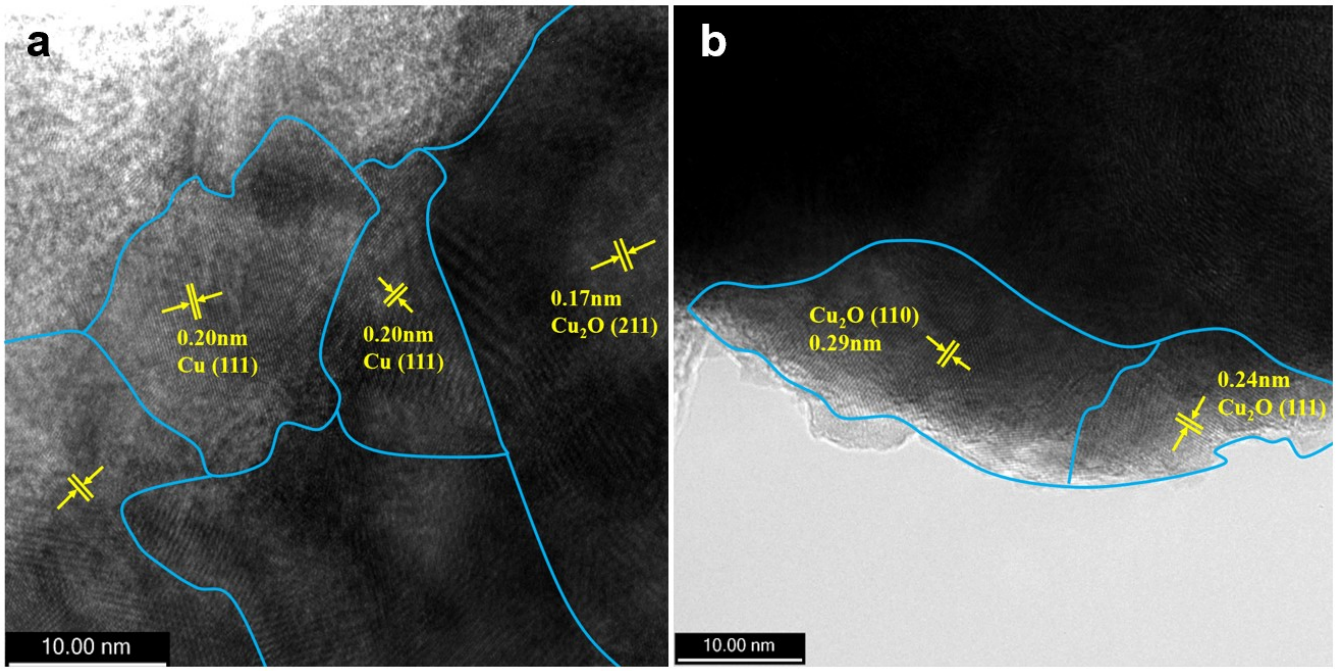

Figure S7. (a-b) HRTEM images of Cu_2O-Ar/H_2 (a) and Cu_2O-Ar/O_2 (b).

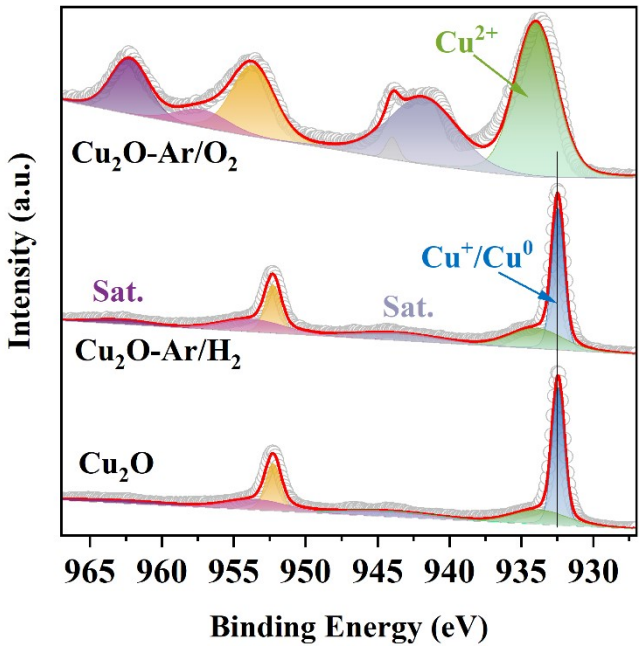

Figure S8. Cu 2p XPS spectra of as-prepared catalysts.

Table S1. Fitted EXAFS parameters at Cu K-edge for Cu_2O, Cu_2O-Ar/H_2, Cu_2O-Ar/O_2, Cu_2O, and CuO reference.

Sample	Path	R-factor	N	R (Å)	σ^2 (Å^2)
CuO reference	Cu-O	5.1	4	1.94±0.008	3.8±1.0
Cu_2O reference	Cu-O	0.0244	2	1.85±0.01	0.003
	Cu-Cu		12	3.03±0.03	0.032
Cu_2O	Cu-O	0.016	1.90	1.84±0.004	0.002
	Cu-Cu		13.1	3.01±0.006	0.032
Cu_2O-Ar/H_2	Cu-O	0.01	1.77	1.79±0.06	0.0019
	Cu-Cu		12.0	2.94±0.06	0.019
Cu_2O-Ar/O_2	Cu-O	0.015	1.65	1.84±0.05	0.001
	Cu-Cu		0.24	2.89±0.03	0.004

N: coordination number; σ^2: mean-square disorder; R-factor: goodness of EXFAS fitting.

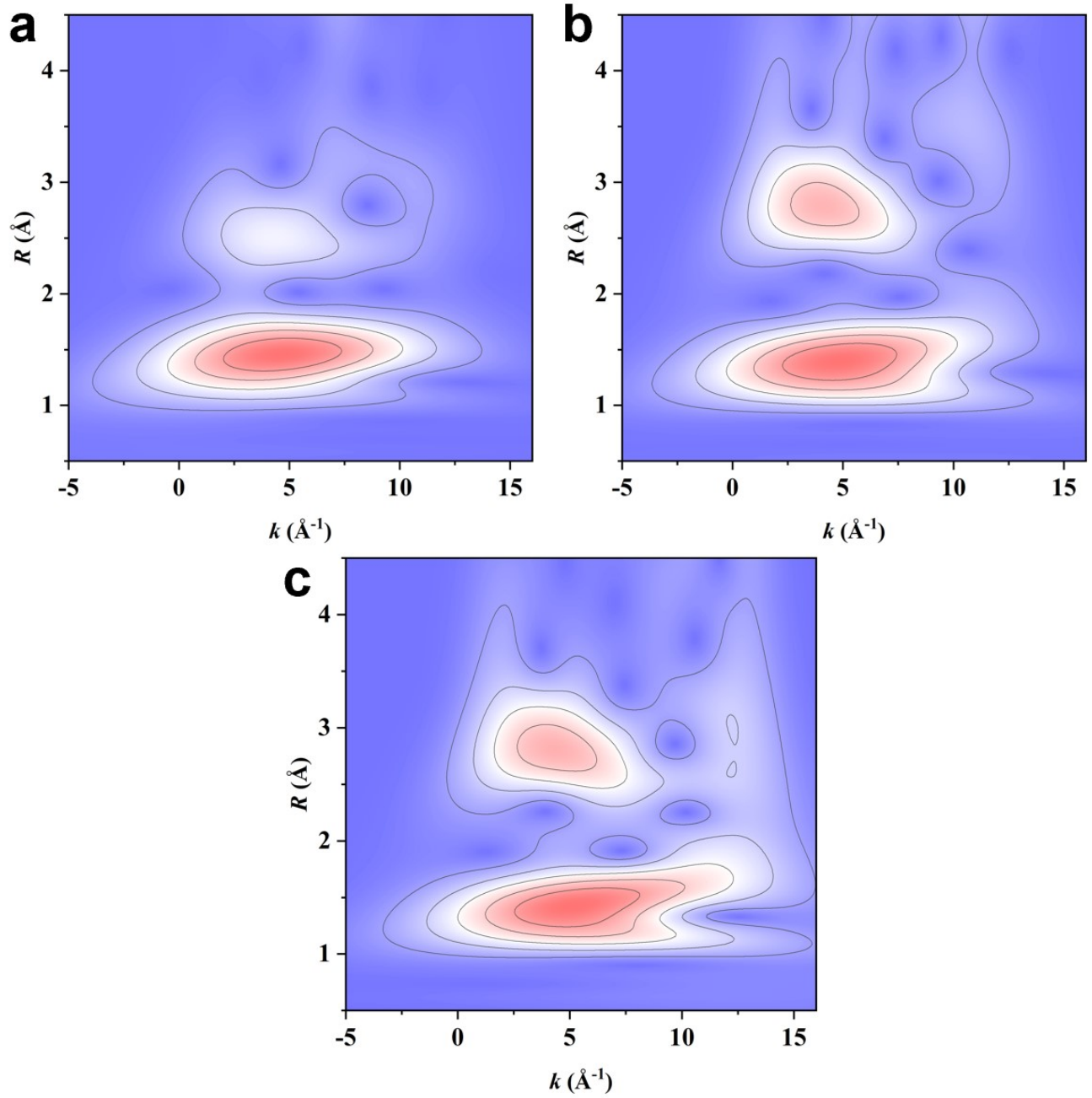

Figure S9. (a-c) Wavelet transforms for the k^3-weighted EXAFS signals of CuO reference (a), original Cu_2O (b), and Cu_2O-Ar/O_2 (c).

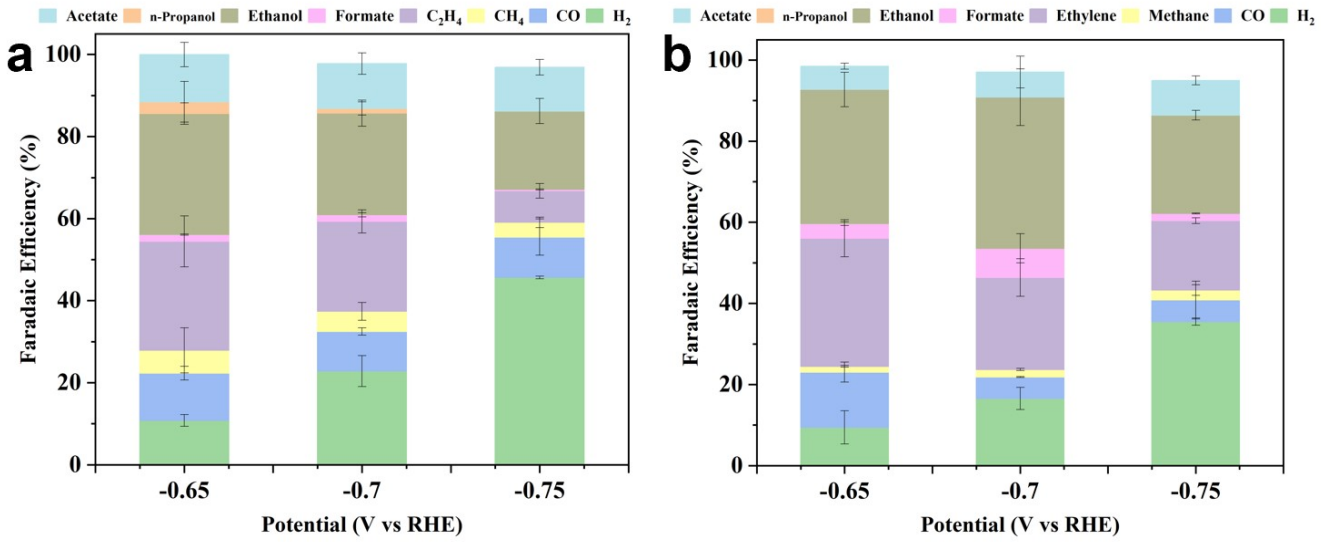

Figure S10. (a-b) The reduced products distribution of CO_2 for Cu_2O (a) and Cu_2O-Ar/O_2 (b) at different cathodic potentials under ECR.

Table S2. The summary of ECR performances for C_{2+} products over various plasma-treated electrocatalysts.

Catalysts	Electrolytes	Reactor	C_{2+} FE (%)	Ref.
Cu_2O-Ar/H_2	1M KOH	Flow cell	81.2	This work
F-Cu	1M KOH	Flow cell	81.6	[1]
Cu_2O(CO)	1M KOH	Flow cell	77.4	[2]
Cu nanocube	0.1M $KHCO_3$	H cell	73	[3]
ON-CuO	0.1M $KHCO_3$	H cell	77	[4]
OD-Cu	0.1M $KHCO_3$	H cell	60	[5]
dendritic Cu	0.1M $KHCO_3$	H cell	45	[6]
Ar_{10min}-plasma Cu	0.1 M $CsHCO_3$	H cell	57.2	[7]
$O_{2,10min}$-plasma Cu	0.1 M $CsHCO_3$	H cell	58.8	[7]

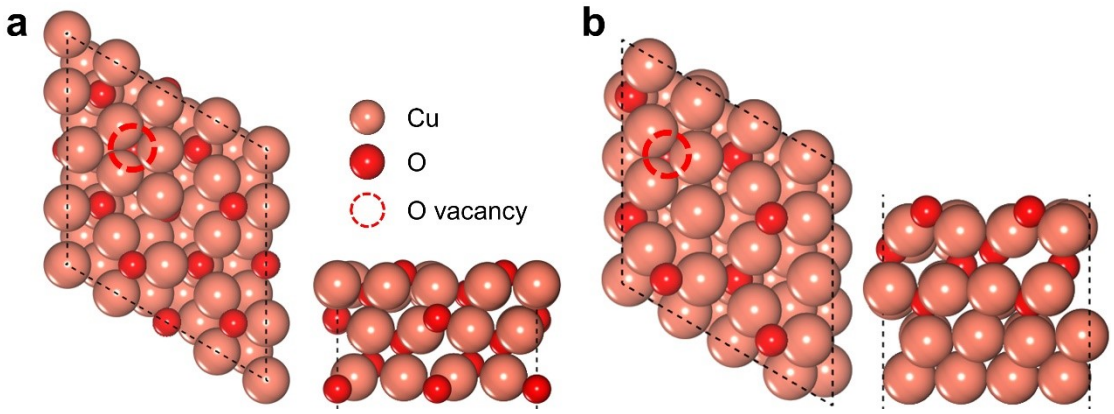

Figure S11. Top and side views of (a) Cu_2O and (b) Cu_2O-Ar/H_2.

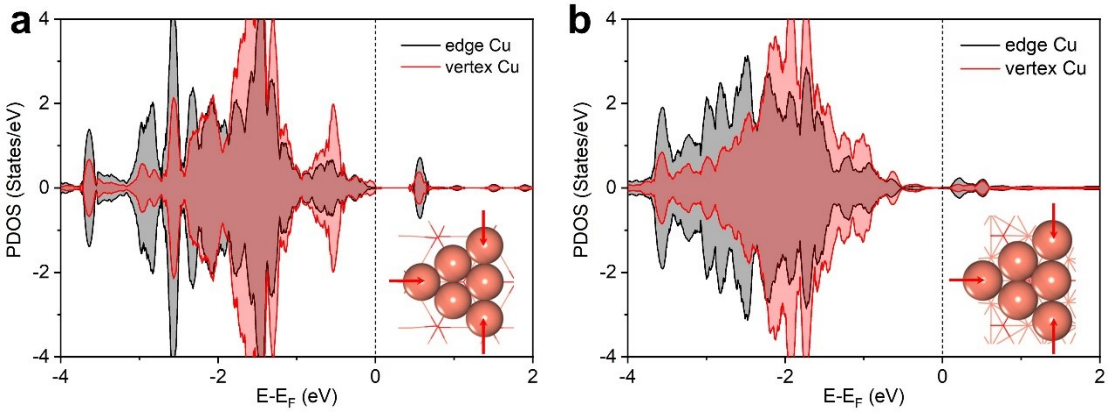

Figure S12. PDOS of vertex and edge Cu atoms of (a) Cu_2O and (b) Cu_2O-Ar/H_2, where red arrows denote vertex atoms.

Table S3. Energies (E) and reaction energies (ΔE) of *CO and *CHO on Cu_2O-Ar/H_2 and Cu_2O with (E_{sol}) and without (E_0) the solvation effect.

	Cu_2O-Ar/H_2		Cu_2O	
	E_0 (eV)	E_{sol} (eV)	E_0 (eV)	E_{sol} (eV)
E_{*CO}	-366.06	-336.60	-343.20	-343.81
E_{*CHO}	-338.80	-339.37	-346.14	-346.78
ΔE_{CHO-CO}	0.65	0.61	0.44	0.42

Reference:

1. Zhou, Z., et al., Enhanced CO2 Electroreduction to Multi-Carbon Products on Copper via Plasma Fluorination. *Adv. Sci.* 2024, 2309963.
2. Wu, Q., et al., Nanograin-Boundary-Abundant Cu2O-Cu Nanocubes with High C2+ Selectivity and Good Stability during Electrochemical CO2 Reduction at a Current Density of 500 mA/cm2. *ACS Nano***.** 2023.
3. Gao, D., et al., Plasma-activated copper nanocube catalysts for efficient carbon dioxide electroreduction to hydrocarbons and alcohols. *ACS Nano***.** 2017**,** *11* (5), 4825-4831.
4. Park, D. G., et al., Increasing CO binding energy and defects by preserving Cu oxidation state via O2-plasma-assisted N doping on CuO enables high C2+ selectivity and long-term stability in electrochemical CO2 reduction. *ACS Catal.* 2023**,** *13* (13), 9222-9233.
5. Mistry, H., et al., Highly selective plasma-activated copper catalysts for carbon dioxide reduction to ethylene. *Nat. Commun.* 2016**,** *7* (1), 1-9.
6. Scholten, F., et al., Plasma-modified dendritic Cu catalyst for CO2 electroreduction. *ACS Catal.* 2019**,** *9* (6), 5496-5502.
7. Jiang, K., et al., Effects of surface roughness on the electrochemical reduction of CO2 over Cu. *ACS Energy Lett***.** 2020**,** *5* (4), 1206-1214.